crystals

MDPI

Article

Comparison of the Nucleation Parameters of Aqueous L-glycine Solutions in the Presence of L-arginine from Induction Time and Metastable-Zone-Width Data

Lie-Ding Shiau [1,2]

[1] Department of Chemical and Materials Engineering, Chang Gung University, Taoyuan 333, Taiwan; shiau@mail.cgu.edu.tw; Tel.: +886-3-2118800 (ext. 5291)
[2] Department of Urology, Linkou Chang Gung Memorial Hospital, Taoyuan 333, Taiwan

Abstract: Induction time and metastable-zone-width (MSZW) data for aqueous L-glycine solutions in the presence of L-arginine impurity were experimentally measured using a turbidity probe in this study. The nucleation parameters, including the interfacial free energy and pre-exponential nucleation factor, obtained from induction time data, were compared with those obtained from MSZW data. The influences of lag time on the nucleation parameters were examined for the induction time data. The effects of L-arginine impurity concentration on the nucleation parameters based on both the induction time and MSZW data were investigated in detail.

Keywords: crystallites; impurities; induction time; metastable zone width; nucleation parameters

check for updates

Citation: Shiau, L.-D. Comparison of the Nucleation Parameters of Aqueous L-glycine Solutions in the Presence of L-arginine from Induction Time and Metastable-Zone-Width Data. *Crystals* **2021**, *11*, 1226. https://doi.org/10.3390/cryst11101226

Academic Editors: Heike Lorenz, Alison Emslie Lewis, Erik Temmel and Jens-Petter Andreassen

Received: 14 September 2021
Accepted: 11 October 2021
Published: 12 October 2021

1. Introduction

In crystal growth, the induction time is defined as the time interval between the establishment of the supersaturated state and the formation of detectable nuclei. The metastable-zone-width (MSZW) limit is defined as the time taken at a given cooling rate between the establishment of the supersaturated state and the formation of detectable nuclei. Nucleation is the initial process for the formation of crystals in liquid solutions. Thus, both the induction time and MSZW data are related to the nucleation rate of the crystallized substance in solutions. In classical nucleation theory (CNT) [1–3], the nucleation rate is expressed in the Arrhenius form, governed by two nucleation parameters, including the interfacial free energy and pre-exponential nucleation factor. The interfacial free energy is the energy required to create a new solid/liquid interface for the formation of crystals in liquid solutions, while the pre-exponential factor is related to the attachment rate of solute molecules to a cluster in the formation of crystals. The influences of impurities on the nucleation parameters have long been investigated using induction time or MSZW data with the addition of different impurities in solutions for a variety of compounds [4–14].

The nucleation parameters of a crystallized substance have been traditionally determined from induction time data by assuming $t_i^{-1} \propto J$, where J is nucleation rate [1]. Recently, various methods have been proposed to calculate the nucleation parameters from MSZW data [15–21]. Although the induction time and MSZW processes are two different temperature-controlling methods for determination of the nucleation parameters in a crystallization system, a model should be available to relate the induction time and MSZW data with the nucleation parameters. Furthermore, as a cooling process is applied first to reach the desired operating temperature and then a constant temperature is adopted in the induction time measurements, there always exists a lag time between the prepared supersaturated solution being at a higher temperature and it being cooled to the desired lower constant temperature. For simplicity, the lag time is usually neglected in determining the nucleation parameters from the induction time data.

The nucleation process can behave differently. For certain systems, induction time cannot even be considered due to sharp phase transition, while for some cases there is

induction time governed by different material properties. For example, by evaporating a cellulose nanocrystal-based cholesteric drop, the drop edges are pinned to the substrate, which leads to nonequilibrium sliding of the individual cholesteric fragment with active ordering [22]; following the induction period of cholesteric collagen tactoids, phase separation goes through the nucleation process during which multiple chiral nuclei spontaneously emerge and grow throughout the continuous isotropic phase [23]. In the present work, a model was proposed based on CNT to relate the induction time and MSZW data with the nucleation parameters for the systems with an experimentally measurable nucleation point. The proposed model was then applied to determine the nucleation parameters for the aqueous L-glycine solutions in the presence of L-arginine impurity from the induction time and MSZW data. The effects of lag time on the nucleation parameters within the induction time data were investigated. L-glycine was adopted in this work as it is the simplest amino acid and is often used as a model compound in the study of solution nucleation [24–30]. L-arginine is another amino acid which was randomly chosen as impurity in the aqueous L-glycine solutions.

2. Theory

The nucleation rate according to CNT is expressed as [1–3]

$$J = A \exp\left[-\frac{16\pi v^2 \gamma^3}{3{k_B}^3 T^3 \ln^2 S}\right], \tag{1}$$

where A is the nucleation pre-exponential factor, γ is the interfacial free energy, k_B is the Boltzmann constant, $v = M_w/\rho_c N_A$ is the molecular volume, T is the temperature, and S is the supersaturation.

A model is derived based on CNT to determine γ and A by relating the induction time and MSZW data with J as follows. If a solution saturated at T_0 is cooled to T_m at a constant cooling rate b within the time period $t = 0$ to t_m and then the temperature is kept at T_m within the time period t_m to $t_m + t_i$, the nucleation event for this combined process is assumed to be detected at $t = t_m + t_i$. If t_m is small compared to t_i, this combined process can be regard as the induction time process with consideration of the lag time t_m, which is the time required for the solution saturated at T_0 to cool to T_m at cooling rate b. Thus, $\Delta T_m = T_0 - T_m$ and the lag time is given by $t_m = \Delta T_m/b$. This combined process for $t_m = 0$ corresponds to the induction time process without consideration of the lag time. On the other hand, this combined process for $t_i = 0$ corresponds to the MSZW process.

Figure 1 depicts the MSZW process for a saturated solution of C_0 cooled at a constant cooling rate b, where T_0 is the initial saturated temperature at $t = 0$, T_m is the nucleation temperature at t_m, C_0 is the saturated concentration at T_0, C_m is the saturated concentration at T_m, $C_{eq}(T)$ is the solubility, and $S(T) = C_0/C_{eq}(T)$ is the supersaturation. As $C_{eq}(T)$ generally decreases with decreasing temperature, $S(T)$ increases and subsequently J increases with time. For the nucleation point at t_m, S_m is the supersaturation at T_m defined as $S_m = C_0/C_{eq}(T_m) = C_0/C_m$. The nucleation rate at T_m is given by

$$J_m = A \exp\left[-\frac{16\pi v^2 \gamma^3}{3{k_B}^3 {T_m}^3 \ln^2 S_m}\right]. \tag{2}$$

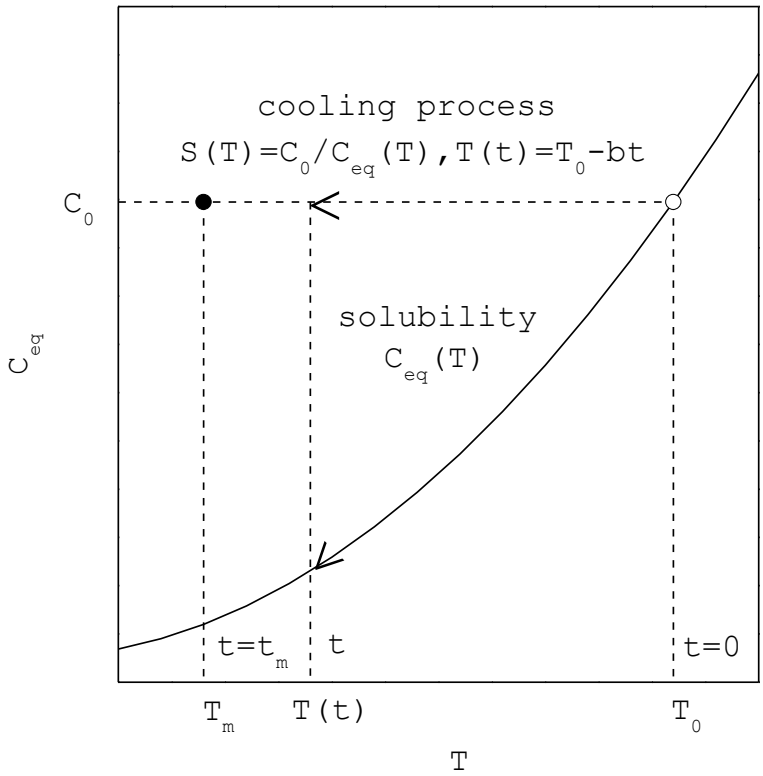

Figure 1. A schematic diagram showing the increasing of supersaturation during the cooling process reproduced from Shiau [31], where $C_{eq}(T)$ is the temperature-dependent solubility (○ represents the starting point and • represents the nucleation point).

Note that both S_m and ΔT_m are measures of the MSZW.

As the first appearance of nuclei can be regarded as a random process, the stochastic process of nucleation can be described by the Poisson's law [32–34]. For the combined process described above, as the temperature is cooled from T_0 to T_m within the time period $t = 0$ to t_m, $S(T)$ increases and J increases with time; and as the temperature is kept at T_m within the time period t_m to $t_m + t_i$, the supersaturation remains the same at S_m and J remains the same at J_m. Based on the given reasoning, the average number of expected nuclei N in a solution volume V within the time period $t = 0$ to $t_m + t_i$ is proposed in this study as

$$N = \left(\int_0^{t_m} JVdt \right) + J_m V t_i \,. \tag{3}$$

where the first term on the right-hand side represents the average number of expected nuclei generated within the time period $t = 0$ to t_m and the second term on the right-hand side represents the average number of expected nuclei generated within the time period t_m to $t_m + t_i$.

Based on the two-point trapezoidal rule for computing the value of a definite integral, one can derive [35]

$$\int_0^{t_m} JVdt = \frac{1}{2}(J_0 + J_m)Vt_m = \frac{J_m V \Delta T_m}{2b} \,, \tag{4}$$

where J_0 and J_m represent the nucleation rate at $t = 0$ and $t = t_m$, respectively. Note that $J_0 = 0$ at $t = 0$ when $S(T_0) = 1$ and $t_m = \Delta T_m / b$.

According to the single nucleus mechanism (SNM) proposed by some researchers through experimental validation [32–34], a single primary nucleus is formed in a supersaturated solution, which grows out to a particular size and undergoes secondary nucleation by

crystal-stirring-impeller or crystal-wall collision. Based on the assumptions that the growth time between the formation of nucleus and growth to the minimum size for secondary nucleation is negligible, and one secondary nucleation is enough to generate detectable crystal volume increase in a negligible amount of time, the nucleation event is detected after the secondary nucleation of the single primary nucleus. Thus, the nucleation event for the combined process occurs at $t = t_m + t_i$ when the first nucleus is formed. By substituting $N = 1$ in Equation (3), combining Equations (2)–(4) leads to

$$\ln\left(\frac{\Delta T_m}{2b} + t_i\right) = -\ln(AV) + \frac{16\pi v^2\gamma^3}{3{k_B}^3{T_m}^3\ln^2 S_m}\,. \tag{5}$$

Thus, Equation (5) can be applied to determine the nucleation parameters from the induction time data, t_i, with consideration of the lag time, $\Delta T_m/b$. A plot of $\ln(\Delta T_m/2b + t_i)$ versus $\ln^2 S_m$ should give a straight line, the slope and intercept of which permit determination of γ and A, respectively.

Equation (5) for $\Delta T_m/b = 0$ reduces to

$$\ln t_i = -\ln(AV) + \frac{16\pi v^2\gamma^3}{3{k_B}^3{T_m}^3\ln^2 S_m}\,, \tag{6}$$

Which corresponds to the conventional method adopted in determination of γ and A from the induction time data without consideration of the lag time. Equation (5) for $t_i = 0$ reduces to

$$\ln\left(\frac{\Delta T_m}{2b}\right) = -\ln(AV) + \frac{16\pi v^2\gamma^3}{3{k_B}^3{T_m}^3\ln^2 S_m}\,, \tag{7}$$

Which can be applied to determine γ and A from the MSZW measurements, where a solution saturated at T_0 is cooled at a constant rate b from $t = 0$ to t_m and the nucleation event is detected at T_m.

If the temperature-dependent solubility is described in terms of the van't Hoff Equation (1), one obtains

$$\ln S_m = \ln\left(\frac{C_0}{C_m}\right) = \frac{-\Delta H_d}{R_G}\left(\frac{1}{T_0} - \frac{1}{T_m}\right) = \left(\frac{\Delta H_d}{R_G T_0}\right)\left(\frac{\Delta T_m}{T_m}\right), \tag{8}$$

where ΔH_d is the heat of dissolution and R_G is the gas constant. Substituting $\ln S_m$ in Equation (8) into Equation (7) yields

$$\left(\frac{T_0}{\Delta T_m}\right)^2 = \frac{3}{16\pi}\left(\frac{k_B T_0}{v^{2/3}\gamma}\right)^3\left(\frac{\Delta H_d}{R_G T_0}\right)^2\left[\ln\left(\frac{\Delta T_m}{b}\right) + \ln\left(\frac{AV}{2}\right)\right]. \tag{9}$$

A plot of $(T_0/\Delta T_m)^2$ versus $\ln(\Delta T_m/b)$ based on the MSZW data should give a straight line, the slope and intercept of which permit determination of γ and A, respectively. Equation (9) is consistent with the result developed by Shiau and Wu [21] in determination of γ and A from the MSZW data.

3. Experimental Methods

Deionized water, L-glycine (>99%, Alfa Aesar) and L-arginine (>98%, ACROS) were used to prepare the desired supersaturated solution for the specified impurity concentration. The experimental apparatus adopted by Shiau and Lu [18] was used in the study of nucleation, which consists of a 250 mL crystallizer equipped with a magnetic stirrer at a constant stirring rate of 350 rpm, immersed in programmable thermostatic water. A turbidity probe with a near-infrared source (Crystal Eyes manufactured by HEL limited, Hertford, UK) was used to detect the nucleation event.

The solubility of L-glycine in water from 303 K to 318 K was measured in this work. The solubility measurements indicated that the solubility of L-glycine in water was nearly not

influenced by the presence of L-arginine ranging from $C_{im} = 0$–10 kg arginine/m^3 solution, which corresponds to 0–0.02 mol arginine/mol glycine. The measured solubility of L-glycine in water was consistent with the solubility data reported by Park et al. [36]. In terms of the van't Hoff equation for the measured solubility, one obtains $\Delta H_d = 10.2$ kJ/mol with $C_{eq}(303\text{ K}) = 215$ kg/m^3 and $C_{eq}(318\text{ K}) = 261$ kg/m^3 in this work.

For the induction time and MSZW experiments, a 200 mL aqueous L-glycine solution $(V = 2 \times 10^{-4}\text{ m}^3)$ at the desired concentration was held at 5 K above the saturated temperature for 20 min to ensure a complete dissolution at the beginning of the experiments, which was also confirmed by the turbidity measurement. In the induction time experiments, the induction time and lag time data were measured by rapidly cooling the supersaturated solution at various supersaturations to 303 K. In the MSZW experiments, MSZW data were measured by cooling the solution saturated at 318 K with different constant cooling rates. Each run was carried out at least three times at each condition for the solubility, the induction time, and the MSZW measurements.

Although L-glycine can be crystallized in different polymorphs, including α-form, β-form and γ-form, α-form is usually obtained from pure aqueous L-glycine solutions [24–30]. In this work, the final dried crystals at the end of the experiments were analyzed using Raman spectroscopy (P/N LSI-DP2-785 Dimension-P2 System, 785 nm, manufactured by Lambda Solutions, INC., Seattle, WA, USA) to validate the polymorph of the L-glycine crystals. By comparing with the Raman spectra of α-form crystals reported by Murli et al. [37], it was found that α-form L-glycine crystals were formed from aqueous L-glycine solutions in this work for various supersaturations without and with the presence of L-arginine impurity. Figure 2 shows some Raman spectra of the L-glycine crystals obtained in this work at $S = 1.07$ and $S = 1.12$ for $C_{im} = 0$ and $C_{im} = 10$ kg/m^3, respectively.

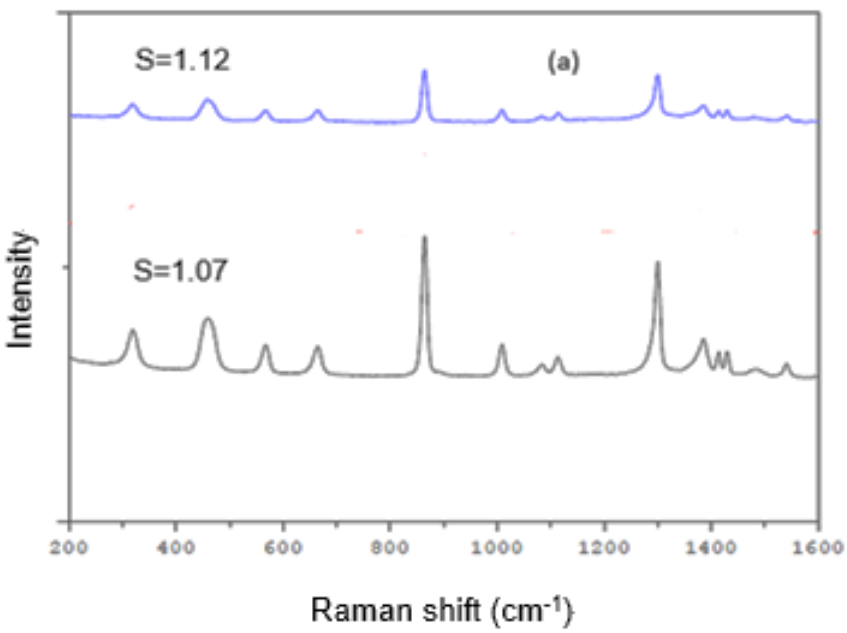

Figure 2. *Cont.*

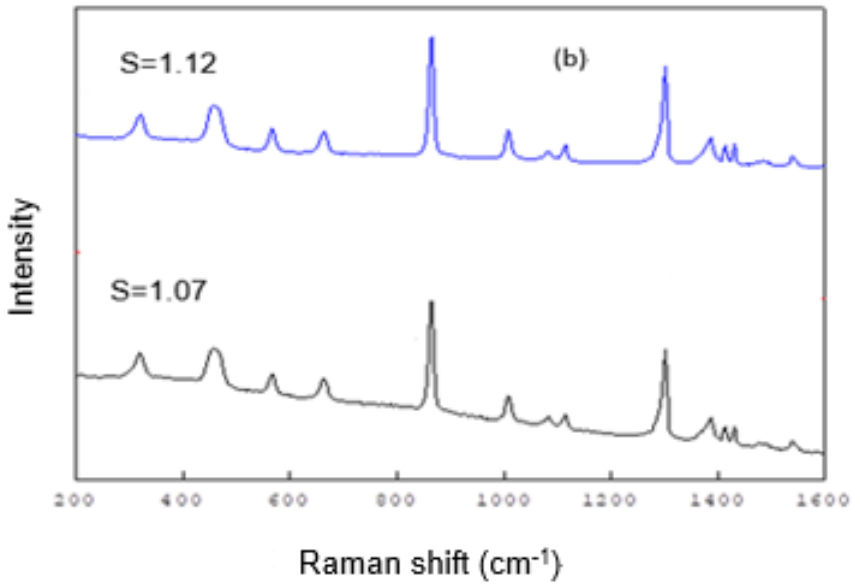

Figure 2. The Raman spectra of the produced L-glycine crystals at $S = 1.07$ and $S = 1.12$ for (**a**) $C_{im} = 0$ and (**b**) $C_{im} = 10$ kg/m^3, respectively.

4. Results and Discussion

The induction time data of aqueous L-glycine solutions were measured for various supersaturations at 303 K in the presence of L-arginine for various impurity concentrations, C_{im}. The average induction times are listed in Table 1. The average lag times for the induction time data are listed in Table 2, which were measured based on $b \cong 0.038$ K/s adopted for cooling the heated supersaturated solution to the desired constant temperature. The lag time corresponds to the time required for the heated solution to be lowered to 303 K. Thus, as the temperature range ΔT_m increases, the lag time increases. The MSZW data of aqueous L-glycine solutions saturated at $T_0 = 318$ K were measured for various b in the presence of L-arginine for $C_{im} = 0$–10 kg/m^3. The average MSZWs are listed in Table 3. Note that $M_w = 0.075$ kg/mol, $\rho_c = 1607$ kg/m^3, and $v = 7.757 \times 10^{-29}$ m^3 for L-glycine.

Table 1. The average induction times, t_i, in the induction time measurements for various impurity concentrations, C_{im}, and supersaturations, S, at 303 K. The standard deviations in the least significant digits are given in parentheses.

C_{im} (kg/m^3)	t_i ($\times 10^2$ s)			
	S = 1.07	**S = 1.08**	**S = 1.10**	**S = 1.12**
0	27 (5.9)	14 (2.8)	8.3 (2.5)	4.4 (2.0)
2	62 (15)	33 (7.3)	16 (4.6)	8.2 (2.5)
5	107 (17)	48 (8.9)	23 (5.1)	12 (3.0)
10	154 (21)	62 (11)	31(8.8)	16(4.7)

Table 2. The average lag time, $\Delta T_m/b$, based on $b \cong 0.038$ K/s in the induction time measurements for various impurity concentrations, C_{im}, and supersaturations, S, at 303 K, where ΔT_m corresponds to the temperature range for a solution with concentration C_0 saturated at T_0 and cooled to 303 K. Note that $\Delta T_m = T_0 - 303$ K and $S = C_0/C_{eq}(303\text{ K})$. The standard deviations in the least significant digits are given in parentheses.

C_{im}(kg/m^3)	$\Delta T_m/b$ (s)			
	S = 1.07 (ΔT_m = 5.1 K)	S = 1.08 (ΔT_m = 5.8 K)	S = 1.10 (ΔT_m = 7.2 K)	S = 1.12 (ΔT_m = 8.7 K)
0	135 (14)	153 (16)	177 (16)	236 (19)
2	127 (12)	144 (13)	195 (17)	221 (17)
5	141 (13)	159 (15)	182 (16)	232 (17)
10	146 (15)	163 (14)	188 (18)	241 (22)

Table 3. The average MSZWs, ΔT_m, in the MSZW measurements for a solution saturated at $T_0 = 318$ K cooled at various impurity concentrations, C_{im}, and cooling rates. The standard deviations in the least significant digits are given in parentheses.

C_{im} (kg/m^3)	ΔT_m(K)			
	b = 0.00417 K/s	b = 0.00833 K/s	b = 0.01111 K/s	b = 0.01389 K/s
0	6.9 (1.6)	8.5 (1.7)	9.1 (2.1)	9.9 (2.2)
2	8.4 (1.8)	10.3 (2.0)	11.7 (2.3)	12.2 (2.3)
5	9.7 (2.1)	12.2 (2.5)	13.8 (2.9)	14.4 (3.1)
10	11.5 (2.3)	13.9 (2.4)	16.1 (2.7)	18.8 (3.3)

Table 1 indicates that t_i increases significantly with increasing C_{im} for each S and decreases with increasing S for each C_{im}. Thus, L-arginine exerts a nucleation inhibition effect in aqueous L-glycine solutions, which increases with increasing C_{im}. Table 2 indicates that $\Delta T_m/b$, increases slightly with increasing S for each C_{im} and remains nearly independent of C_{im}. Note that ΔT_m corresponds to the temperature range for a solution saturated at T_0 cooled to 303 K, where T_0 increases with increasing S and remains nearly independent of C_{im}. For example, $\Delta T_m/b = 236$ s is quite significant compared with $t_i = 442$ s at $S = 1.12$ ($\Delta T_m = 8.7$ K) for $C_{im} = 0$. On the other hand, $\Delta T_m/b = 135$ s is negligible compared with $t_i = 2672$ s at $S = 1.07$ ($\Delta T_m = 5.1$ K) for $C_{im} = 0$.

Figure 3 shows plots of $\ln t_i$ against $\ln^2 S_m$ for each C_{im} according to Equation (6) based on the induction time data without consideration of the lag time. Figure 4 shows plots of $\ln(\Delta T_m/2b + t_i)$ against $\ln^2 S_m$ for each C_{im} according to Equation (5) based on the induction time data with consideration of the lag time. Calculated values of γ and A from the slope and intercept of the best-fit plots for each C_{im} are listed in Table 4. Note that the regression coefficient, R^2, with the lag time is generally greater than that without the lag time for each C_{im}, which indicates that Equation (5) with the lag time fits the induction time data better than Equation (6) without the lag time.

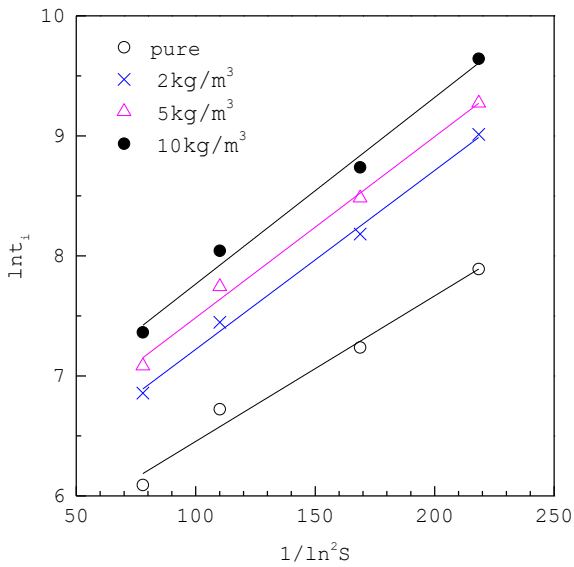

Figure 3. Plots of $\ln t_i$ against $\ln^2 S_m$ for various impurity concentrations, C_{im}, according to Equation (6) based on the induction time data without consideration of the lag time.

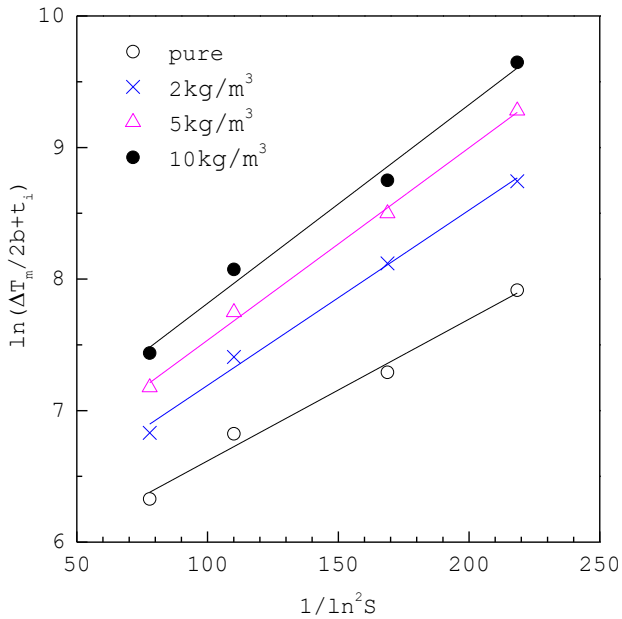

Figure 4. Plots of $\ln(\Delta T_m/2b + t_i)$ against $\ln^2 S_m$ for various impurity concentrations, C_{im}, according to Equation (5) based on the induction time data with consideration of the lag time.

Table 4. Calculated values of γ and A with the regression coefficients, R^2, based on the induction time data. The number before the slash represents the value without consideration of the lag time and the number after the slash represents the value with consideration of the lag time.

C_{im} (kg/m^3)	γ (mJ/m^2)	A (m^{-3}s^{-1})	R^2
0	2.07/1.99	26.5/19.7	0.981/0.987
2	2.17/2.13	16.9/14.3	0.991/0.994
5	2.22/2.20	12.7/11.6	0.993/0.997
10	2.24/2.22	10.0/9.1	0.989/0.990

As indicated in Table 4, one can note that the value of γ with the lag time, γ_{lag}, is lower by about 2% than that without the lag time, γ, while the value of A with the lag time,

A_{lag}, is lower by about 15% than that without the lag time, A. These findings are consistent with $\gamma_{lag} < \gamma$ and $A_{lag} < A$ derived in Supplementary Materials.

Table 3 indicates that ΔT_m increases with increasing C_{im} for each b and increases with increasing b for each C_{im}. Thus, as similar to the results from the induction time data, L-arginine exerts a nucleation inhibition effect in aqueous L-glycine solutions, which increases with increasing C_{im}. Figure 5 shows plots of $(T_0/\Delta T_m)^2$ against $\ln(\Delta T_m/b)$ for various C_{im} according to Equation (9) based on the MSZW data. Calculated values of γ and A from the slope and intercept of the best-fit plots for each C_{im} are listed in Table 5.

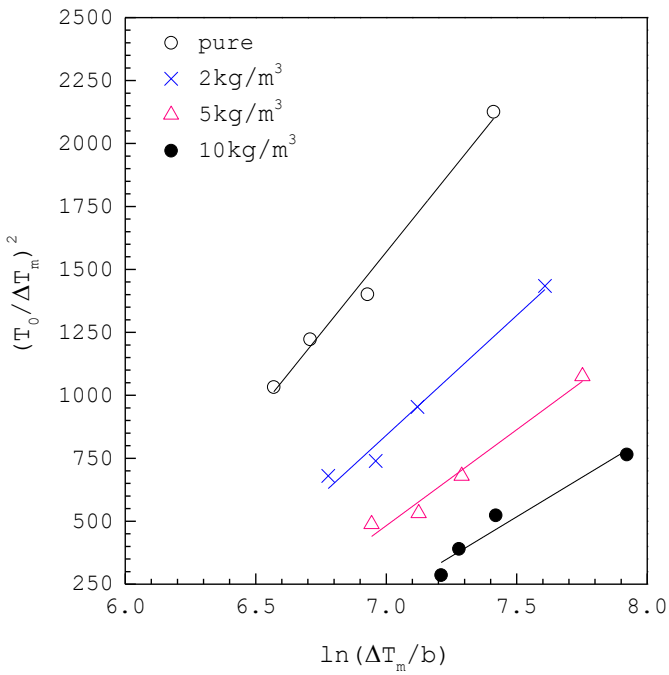

Figure 5. Plots of $(T_0/\Delta T_m)^2$ against $\ln(\Delta T_m/b)$ for various impurity concentrations, C_{im}, according to Equation (9) based on the MSZW data.

Table 5. Calculated values of γ and A with the regression coefficients, R^2, based on the MSZW data.

C_{im} (kg/m^3)	γ (mJ/m^2)	A (m^{-3}s^{-1})	R^2
0	2.13	30.9	0.990
2	2.36	22.1	0.981
5	2.54	17.2	0.975
10	2.71	12.6	0.953

The values of γ and A obtained from the MSZW data in Table 5 are consistent with those obtained from the induction time data in Table 4. They all indicate that, as C_{im} increases, γ increases slightly while A decreases quite significantly. For example, as C_{im} increases from 0 to 10 kg/m^3, γ only increases slightly in the range of 10% to 30%, while A decreases significantly in the range of 50% to 60%. It is speculated that the presence of L-arginine in the aqueous L-glycine solution leads to some L-arginine molecules adsorbed on the nucleus surface of L-glycine, which suppresses nucleation and results in a higher γ compared to that without L-arginine adsorbed on the nucleus surface of L-glycine. On the other hand, the presence of L-arginine in the aqueous L-glycine solution suppresses nucleation and results in a lower A compared to that without L-arginine in the aqueous L-glycine solution. As the effects of L-arginine impurity on γ and A become more profound at a greater concentration of L-arginine impurity, a greater C_{im} results in a higher γ and a lower A. This trend is consistent with the finding reported by Heffernan et al. [8] for the

nucleation of curcumin in propan-2-ol due to the presence of demethoxycurcumin and bisdemethoxycurcumin.

5. Conclusions

A model was proposed based on CNT to determine the nucleation parameters from both the induction and MSZW data. The unique feature is that the derivation of this model for both the induction and MSZW data is based on the same assumption that the nucleation point corresponds to the formation of a single primary nucleus in a supersaturated solution. This model results in two different equations. One is derived for the induction data while the other is derived for the MESZW data. The proposed model was applied to calculate the interfacial free energy and pre-exponential nucleation factor from both the induction time data and the MSZW data for the aqueous L-glycine solutions in the presence of L-arginine impurity. The results indicated that the values of interfacial free energy and pre-exponential nucleation factor obtained from the MSZW data are consistent with those obtained from the induction time data. The induction time data with consideration of the lag time lead to a lower interfacial free energy and a lower pre-exponential nucleation factor than those for the induction time data without consideration of the lag time. As the impurity concentration increases, the interfacial free energy increases slightly while the pre-exponential nucleation factor decreases quite significantly based on both the induction time and MSZW data.

Supplementary Materials: The following are available online at https://www.mdpi.com/article/10.3390/cryst11101226/s1, The derivation of $\gamma_{lag} < \gamma$ and $A_{lag} < A$.

Funding: This research was funded by Chang Gung Memorial Hospital (CMRPD2K0012) and Ministry of Science and Technology of Taiwan (MOST108-2221-E-182-034-MY2).

Data Availability Statement: Not applicable.

Acknowledgments: The author would like to thank Chang Gung Memorial Hospital (CMRPD2K0012) and Ministry of Science and Technology of Taiwan (MOST108-2221-E-182-034-MY2) for financial support of this research. The author also expresses his gratitude to Pin-Jhu Li and Dai-Rong Wu for their experimental work.

Conflicts of Interest: The authors declare no conflict of interest.

Notation

A = pre − exponential nucleation factor $(\mathrm{m}^{-3}\mathrm{s}^{-1})$
b = cooling rate (K/s)
C_0 = initial saturated concentration at T_0 $(\mathrm{kg/m}^3)$
$C_{eq}(T)$ = saturated concentration at $T(\mathrm{kg/m}^3)$
C_m = saturated concentration at T_m $(\mathrm{kg/m}^3)$
C_{im} = concentration of impurity $(\mathrm{kg/m}^3)$
J = nucleation rate $(\mathrm{m}^{-3}\mathrm{s}^{-1})$
J_0 = nucleation rate at $t = 0$ $(\mathrm{m}^{-3}\mathrm{s}^{-1})$
J_m = nucleation rate at t_m $(\mathrm{m}^{-3}\mathrm{s}^{-1})$
k_B = Boltzmann constant $(= 1.38 \times 10^{-23}\ \mathrm{J/K})$
M_W = molar mass (kg/mol)
N = average number of expected nuclei $(-)$
N_A = Avogadro number $\left(= 6.02 \times 10^{23}\ \mathrm{mol}^{-1}\right)$
R_G = gas constant $\left(= 8.314\ \mathrm{J\ mol}^{-1}\mathrm{K}^{-1}\right)$
S = supersaturation $(-)$
S_m = supersaturation at t_m $(-)$
T = temperature (K)
T_0 = initial saturated temperature (K)
T_m = temperature at t_m (K)
t = time (s)

t_i = induction time (s)
t_m = time at the MSZW limit (s)
V = solution volume (m^3)
Greek Letters
ρ_c = crystal density (kg/m^3)
v = volume of the solute molecule (m^3)
γ = interfacial free energy (J/m^2)
ΔH_d = heat of dissolution (J/mole)
ΔT_m = MSZW (K)

References

1. Mullin, J.W. *Crystallization*, 3rd ed.; Butterworth-Heinemann: Oxford, UK, 1993.
2. Kashchiev, D. *Nucleation: Basic Theory with Applications*; Butterworth-Heinemann: Oxford, UK, 2000.
3. Kashchiev, D.; van Rosmalen, G.M. Review: Nucleation in solutions revisited. *Cryst. Res. Technol.* **2003**, *38*, 555–574. [CrossRef]
4. Dhanasekaran, P.; Srinivasan, P. Nucleation control, separation and bulk growth of metastable α-L-glutamic acid single crystals in the presence of L-tyrosine. *J. Cryst. Growth.* **2013**, *364*, 23–29. [CrossRef]
5. Peng, J.; Dong, Y.; Wang, L.; Li, L.L.; Li, W.; Feng, H. Effect of impurities on the solubility, metastable zone width, and nucleation kinetics of borax decahydrate. *Ind. Eng. Chem. Res.* **2014**, *53*, 12170–12178. [CrossRef]
6. Siepermann, C.A.P.; Huang, S.; Myerson, A.S. Nucleation inhibition of benzoic acid through solution complexation. *Cryst. Growth Des.* **2017**, *17*, 2646–2653. [CrossRef]
7. Yang, L.; Cao, J.; Luo, T. Effect of Mg^{2+}, Al^{3+}, and Fe^{3+} ions on crystallization of type α hemi-hydrated calcium sulfate under simulated conditions of hemi-hydrate process of phosphoric acid. *J. Cryst. Growth* **2018**, *486*, 30–37. [CrossRef]
8. Heffernan, C.; Ukrainczyk, M.; Zeglinski, J.; Hodnett, B.K.; Rasmuson, A.C. Influence of structurally related impurities on the crystal nucleation of curcumin. *Cryst. Growth Des.* **2018**, *18*, 4715–4723. [CrossRef]
9. Su, N.; Wang, Y.; Xiao, Y.; Lu, H.; Lou, Y.; Huang, J.; He, J.; Li, Y.; Hao, H. Mechanism of influence of organic impurity on crystallization of sodium sulfate. *Ind. Eng. Chem. Res.* **2018**, *57*, 1705–1713. [CrossRef]
10. Bodnar, K.; Hudson, S.P.; Rasmuson, A.C. Promotion of mefenamic acid nucleation by a surfactant additive, docusate sodium. *Cryst. Growth Des.* **2019**, *19*, 591–603. [CrossRef]
11. Keshavarz, L.; Steendam, R.R.E.; Blijlevens, M.A.R.; Pishnamazi, M.; Frawley, P.J. Influence of impurities on the solubility, nucleation, crystallization, and compressibility of paracetamol. *Cryst. Growth Des.* **2019**, *19*, 4193–4201. [CrossRef]
12. Huang, Y.; Lu, J.; Chen, H.; Du, W.; Wang, X. Effects of succinic acid and adipic acid on the metastable width of glutaric acid in acetic acid. *J. Cryst. Growth.* **2019**, *507*, 1–9. [CrossRef]
13. Chen, J.; Peng, J.; Wang, X.; Dong, Y.; Li, W. Effects of CO_3^{2-} and OH^- on the solubility, metastable zone width and nucleation kinetics of borax decahydrate. *R. Soc. Open Sci.* **2019**, *6*, 181862. [CrossRef]
14. Luo, M.; Liu, C.; Song, X.; Yu, J. Effects of $Al_2(SO_4)_3$ and K_2SiO_3 impurities on the crystallization of K_2SO_4 from aqueous solutions. *Cryst. Res. Technol.* **2021**, *56*, 2000052. [CrossRef]
15. Kubota, N. A new interpretation of metastable zone widths measured for unseeded solutions. *J. Cryst. Growth* **2008**, *310*, 629–634. [CrossRef]
16. Sangwal, K. Effects of impurities on the metastable zone width of solute-solvent systems. *J. Cryst. Growth* **2009**, *311*, 4050–4061. [CrossRef]
17. Shiau, L.D.; Lu, T.S. A model for determination of the interfacial energy from the measured metastable zone width by the polythermal method. *J. Cryst. Growth* **2014**, *402*, 267–272. [CrossRef]
18. Shiau, L.D.; Lu, T.S. A model for determination of the interfacial energy from the induction time or metastable zone width data based on turbidity measurements. *CrystEngComm* **2014**, *16*, 9743–9752. [CrossRef]
19. Yang, H.; Florence, A.J. Relating induction time and metastable zone width. *CrystEngComm* **2017**, *19*, 3966–3978. [CrossRef]
20. Li, Z.; Si, A.; Yan, Y.; Zhang, X.; Yang, H. Interaction of metastable zone width and induction time based on nucleation potential. *Ind. Eng. Chem. Res.* **2020**, *59*, 22597–22604.
21. Shiau, L.D.; Wu, D.R. Effect of L-valine impurity on the nucleation parameters of aqueous L-glutamic acid solutions from metastable zone width. *J. Cryst. Growth* **2020**, *546*, 125790. [CrossRef]
22. Chu, G.; Vilensky, R.; Vasilyev, G.; Martin, P.; Zhang, R.; Zussman, E. Structure evolution and drying dynamics in sliding cholesteric cellulose nanocrystals. *J. Phys. Chem. Lett.* **2018**, *9*, 1845–1851. [CrossRef]
23. Khadem, S.A.; Rey, A.D. Nucleation and growth of cholesteric collagen tactoids: A time-series statistical analysis based on integration of direct numerical simulation (DNS) and long short-term memory recurrent neural network (LSTM-RNN). *J. Colloid Interface Sci.* **2021**, *582*, 859–873. [CrossRef] [PubMed]
24. Towler, C.S.; Davey, R.J.; Lancaster, R.W.; Price, C.J. Impact of molecular speciation on crystal nucleation in polymorphic systems: the conundrum of γ glycine and molecular 'self-poisoning'. *J. Am. Chem. Soc.* **2004**, *126*, 13347–13353. [CrossRef] [PubMed]
25. Sun, X.; Garetz, B.A.; Myerson, A.S. Supersaturation and polarization dependence of polymorph control in the nonphotochemical laser-induced nucleation(NPLIN) of aqueous glycine solutions. *Cryst. Growth Des.* **2006**, *6*, 684–689. [CrossRef]

26. Bouchard, A.; Hofland, G.W.; Witkamp, G.J. Solubility of glycine polymorphs and recrystallization of β-glycine. *J. Chem. Eng. Data* **2007**, *52*, 1626–1629. [CrossRef]
27. Srinivasan, P.; Indirajith, R.; Gopalakrishnan, R. Growth and characterization of α and γ-glycine single crystals. *J. Cryst. Growth* **2011**, *318*, 762–767. [CrossRef]
28. Han, G.; Chow, P.S.; Tan, R.B.H. Direct comparison of α- and γ-glycine growth rates in acidic and basic solutions: New insights into glycine polymorphism. *Cryst. Growth Des.* **2012**, *12*, 2213–2220. [CrossRef]
29. Yani, Y.; Chow, P.S.; Tan, R.B.H. Glycine open dimers in solution: New insights into α-glycine nucleation and growth. *Cryst. Growth Des.* **2012**, *12*, 4771–4778. [CrossRef]
30. Devi, K.R.; Srinivasan, K. A novel approach to understand the nucleation kinetics of α and γ polymorphs of glycine from aqueous solution in the presence of a selective additive through charge compensation mechanism. *CrystEngComm* **2014**, *16*, 707–722. [CrossRef]
31. Shiau, L.D. Comparison of the interfacial energy and pre-exponential factor calculated from the induction time and metastable zone width data based on classical nucleation theory. *J. Cryst. Growth* **2016**, *450*, 50–55. [CrossRef]
32. Jiang, S.; ter Horst, J.H. Crystal nucleation rates from probability distributions of induction times. *Cryst. Growth Des.* **2011**, *11*, 256–261. [CrossRef]
33. Kadam, S.S.; Kramer, H.J.M.; ter Horst, J.H. Combination of a single primary nucleation event and secondary nucleation in crystallization processes. *Cryst. Growth Des.* **2011**, *11*, 1271–1277. [CrossRef]
34. Kadam, S.S.; Kulkarni, S.A.; Coloma Ribera, R.; Stankiewicz, A.I.; ter Horst, J.H. A new view on the metastable zone width during cooling crystallization. *Chem. Eng. Sci.* **2012**, *72*, 10–19. [CrossRef]
35. Green, D.W.; Perry, R.H. *Perry's Chemical Engineers' Handbook*, 8th ed.; McGraw Hill Book Company: New York, NY, USA, 2008.
36. Park, K.; Evans, J.M.B.; Myerson, A.S. Determination of Solubility of Polymorphs Using Differential Scanning Calorimetry. *Cryst. Growth Des.* **2003**, *3*, 991–995. [CrossRef]
37. Murli, C.; Thomas, S.; Venkateswaran, S.; Sharma, S.M. Raman spectroscopic investigation of α-glycine at different temperatures. *Phys. B* **2005**, *364*, 233–238. [CrossRef]